Transducer Geometry Imperfection Compensation

Tomov, Borislav Gueorguiev; Bhatti, Mudabbir Tufail; Yiu, Billy; Diederichsen, Søren Elmin; Thomsen, Erik Vilain; Jensen, Jørgen Arendt

Published in:
Proceedings of SPIE

Publication date:
2025

Document Version
Peer reviewed version

Transducer Geometry Imperfection Compensation

Borislav Gueorguiev Tomov[1], Mudabbir Tufail Bhatti[1], Billy Yat Shun Yiu[1], Søren Elmin Diederichsen[2], Erik Vilain Thomsen[2], and Jørgen Arendt Jensen[1]

[1]Center for Fast Ultrasound Imaging, Department of Health Technology, Technical University of Denmark, 2800 Kongens Lyngby, Denmark
[2]MEMS Applied Sensors Group, Department of Health Technology, Technical University of Denmark, 2800 Kongens Lyngby, Denmark

ABSTRACT

Multi-element ultrasound arrays are not always perfect, especially when produced using experimental technology. Element variability leads to deterioration of image quality, which prevents a fair comparison to more established transducer manufacturing technologies. This paper presents an approach to compensate for the geometric (Z-axis) imperfections of a transducer, relying on the characterization results of its individual elements. It is hypothesized that compensating for the geometric imperfection of the transducer can significantly improve the ultrasound image quality. The potential of the approach is evaluated through image quality comparison using a commercial transducer, an experimental transducer, and a multi-wire phantom. For a wire at 75 mm depth, the lateral width of a wire image is reduced from 7.4 λ to 3.1 λ, and the cystic contrast ($r = 2.5\lambda$) is improved from -21.4 dB to -31.1 dB.

Keywords: ultrasound, imaging, beamforming, transducer, imperfection, correction, calibration

1. INTRODUCTION

When using multi-element ultrasound transducer arrays, perfect operation by each element is usually assumed. This may not always be the case, especially when the array has been manufactured using an experimental fabrication technique, which may be otherwise promising with respect to transducer performance (bandwidth, efficiency, sensitivity, etc.). The imperfections manifest themselves as errors in position, non-uniform sensitivity, and non-uniform frequency response of the individual transducer elements [1]. Additionally, for multi-part (multi-panel) transducer arrays, such as, for example, 2D matrix arrays, the individual panels may be laterally displaced, tilted, and rotated by various degrees [2]. The imperfections lead to degraded focusing, and the loss of image quality makes the evaluation of new transducer technologies or imaging techniques, as well as the general use of imperfect transducers, more difficult. This paper presents a technique for compensating the geometric (Z-axis) imperfections of transducers, which uses the output of a previously proposed transducer characterization method [1]. The performance of the compensation approach is evaluated through phantom measurements and image quality comparisons by estimating resolution and contrast with and without compensation.

2. METHODS

2.1 Transducer characterization

An ultrasound transducer is characterized by estimating the performance of each of its elements. This is done through emissions into a hydrophone for evaluating the transmit performance and into a reflective plate to estimate the transmit-receive performance [1]. Among the results of a characterization procedure are tables with relative strength and relative signal delay per element.

Further author information: (Send correspondence to B.G.T.)
B.G.T.: E-mail: bgto@dtu.dk, Telephone: +45 45253665
M.T.B.: E-mail: mutu@dtu.dk, Telephone: +45 45255256
B.Y.S.Y: E-mail: yshyi@dtu.dk
S.E.D.: E-mail: seldi@nanotech.dtu.dk
E.V.T: E-mail: ervt@dtu.dk
J.A.J.: E-mail: jaje@dtu.dk, Telephone: +45 45253924

	CMUT	PZT	Unit
Type	Linear	Linear	
No. elements	192	192	
Pitch	0.2	0.2	mm
Centre frequency (stated)	5	4.8	MHz
Height	6	6	mm
Elevation focus	38	38	mm
Bandwidth	80%	60%	

Table 1: Probe Parameters

2.2 Beamformer correction

The beamformer that is used allows calculation of time of flight for arbitrary transducer geometry [3]. The relative signal delays per element, estimated during transducer characterization, are converted to distances along the Z axis (image depth) and are set as Z coordinates of the transducer elements instead of the default (ideal) zeros. The modified transducer model geometry is used in both calculating the transmit delays for the individual sub-aperture elements in the virtual sources and in the beamforming of the incoming echo signals.

2.3 Experimental setup

The method has been implemented on the Verasonics Vantage 256 scanner (Verasonics, Inc., Kirkland, WA, USA) [4], controlled by Matlab (MathWorks, Natick, MA, USA). An experimental 4.8 MHz 192-element linear array capacitive micro-machined ultrasonic transducer (CMUT) [5] and a commercial linear array transducer with the same element geometry and pitch have been used.

2.3.1 Transmit field measurement

The transmit field measurement is performed in an Onda AIMS III system (Onda Corporation, Sunnyvale, CA, USA), using an Onda HGL0400 hydrophone, Onda ATH2000 attenuator, Onda AH2010 preamplifier and a Picoscope 5244D USB oscilloscope (Pico Technology Ltd., Cambridgeshire, United Kingdom), triggered by a Verasonic Vantage 256 scanner, both set up and controlled by a Matlab program. The transducer is fixed in a 3D-printed adapter, and the hydrophone is aligned to it using the procedure described in [1], so that the hydrophone movement is done in a transducer-centric coordinate system.

A focused transmit beam is emitted from the center of the CMUT straight down by Hanning-window apodized 64-element aperture toward a focal point at 38 mm depth, with F#=3. The pressure field is scanned on a grid that covers both the focal point and the point with the peak pressure of the beam. This is done for both uncorrected (Z=0) and corrected element coordinates in the transducer model.

A similar experiment is then performed using an aperture of 32 elements at one edge of the transducer, centered at 16 mm away from the middle of the transducer sole, focused at the same depth as above. In that case, the beam has F#=6.

The direction and maximum pressure of the beams are compared with and without transducer geometry compensation.

2.3.2 Phantom measurement

The imaging sequence is a synthetic aperture scan comprising 12 divergent emissions from sub-apertures of 32 elements [6]. A single-cycle sinusoidal excitation at 4.8 MHz was used. The imaged object is a multi-wire phantom comprising 1 row of wires, with a saw-tooth rubber floor, starting at around 120 mm depth.

The image quality is evaluated through the measured parameters of the images of the phantom wires. The measured parameters are:

- lateral span of the wire images at -6 dB relative level,
- axial span of the wire images at -6 dB relative level,
- cystic contrast as defined in [7], for cyst radius of 2.5 λ.

3. RESULTS

The transducer is an early generation CMUT and has a manufacturing process-induced curvature where the center protrudes by 0.4 mm (1.3 λ) compared to the outer elements, as indicated by the relative signal delay table (Fig. 1) from the transducer characterization.

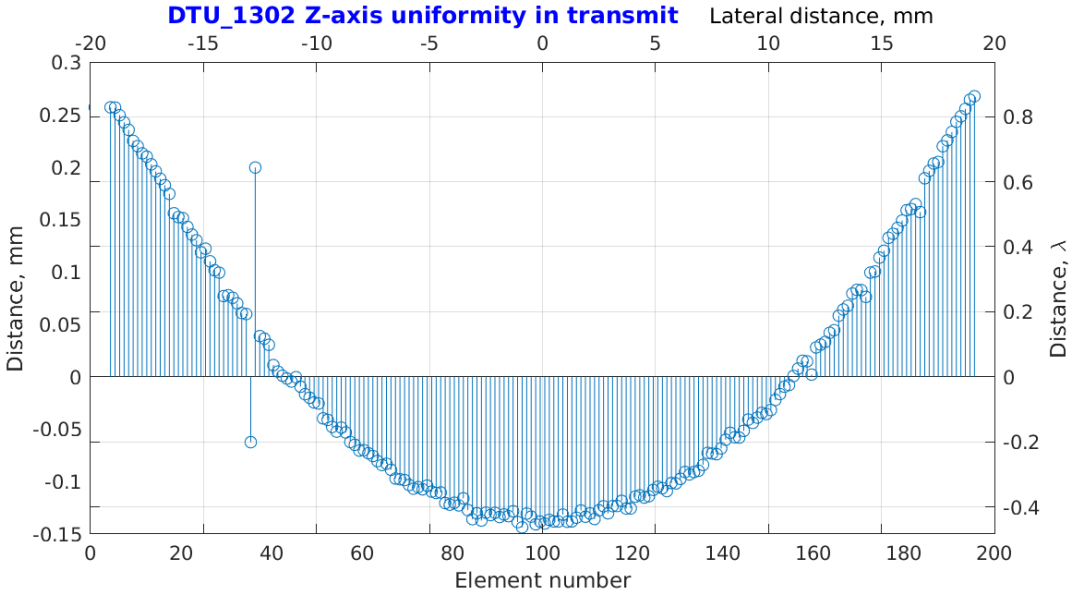

Figure 1: Transmit delay deviations, estimated during transducer characterization.

3.1 Transmit field

The pressure field for the focused ultrasound beam from the center sub-aperture is shown in Fig. 2. The maximum pressure changes from 2.84 MPa without correction to 2.92 MPa with correction.

The pressure field for the focused ultrasound beam from the edge sub-aperture is shown in Fig. 3. The maximum pressure changes from 1.38 MPa without correction to 1.41 MPa with correction. The lower pressure is expected since there are twice fewer elements used in transmit.

It can be observed that, due to the nature of the transducer geometry imperfections (gradual, symmetric), the center beam is not noticeably distorted. Still, the coherence of the contributing individual spherical waves is not perfect, hence the slight increase of 3 % in maximum pressure.

The edge beam has a distinct tilt, which, if uncorrected, would lead to geometric distortion and deteriorated beamforming in an image. With transducer geometry compensation, the direction of the beam is largely corrected, and it gains 2.1 % in maximum pressure.

3.2 Imaging

Fig. 4 shows acquired and beamformed images of the first 4 wires of the wire phantom without and with delay correction, presented with a dynamic range of 60 dB.

Fig. 5 shows a contour plot of the images of the 3rd wire (at 75 mm), created using the commercial transducer without and with delay correction.

Fig. 6 shows a contour plot of the images of the 3rd wire (at 75 mm), created using the experimental transducer without and with delay correction.

Tables 2, 3, and 4 summarize the image quality metrics for the images of the 4 wires of the utilized phantom. The abbreviation XDC means "transducer".

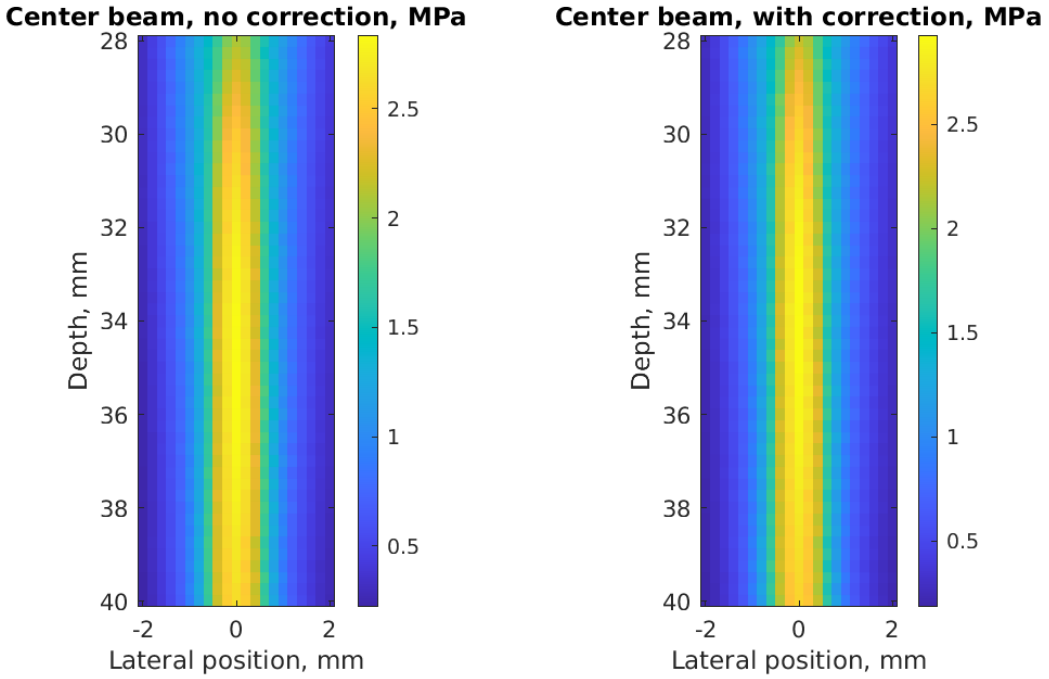

(a) (b)

Figure 2: Transmit delay deviations, measured during transducer characterization.

	Wire at 28 mm	Wire at 50 mm	Wire at 75 mm	Wire at 100 mm
Comm. XDC, default	1.74	1.93	2.47	3.20
Comm. XDC, corrected	1.68	1.84	2.40	3.13
Exp. XDC, default	2.99	5.25	7.41	9.63
Exp XDC, corrected	2.28	2.40	3.09	4.05

Table 2: Lateral PSF width (in lambda, 4.8 MHz)

The lateral PSF and the contrast improve with both transducers by compensation, but on the commercial transducer, the imperfections are much smaller, so the gain is also much less dramatic.

It is worth noting that the axial PSF spans of the wire images made by the experimental transducer are shorter because that transducer has a slightly larger bandwidth.

4. DISCUSSION

In this work, we have proposed a framework that can identify and compensate for the imperfection in the transducer geometry to recover both the transmit beam profile and image quality. The framework characterized the transducer geometry by measuring its pulse-echo time for a planar reflector. The difference in time delay was then translated into geometrical errors of the transducer model. With the corrected transducer geometry, the transmit beam profile was recovered (see Figure 3), as well as the image quality (see Figure 4). The framework

	Wire at 28 mm	Wire at 50 mm	Wire at 75 mm	Wire at 100 mm
Comm. XDC, default	1.00	1.10	1.13	1.17
Comm. XDC, corrected	1.00	1.10	1.14	1.18
Exp. XDC, default	0.91	0.94	1.03	1.04
Exp XDC, corrected	0.91	0.93	0.98	0.92

Table 3: Axial PSF span (in lambda, 4.8 MHz)

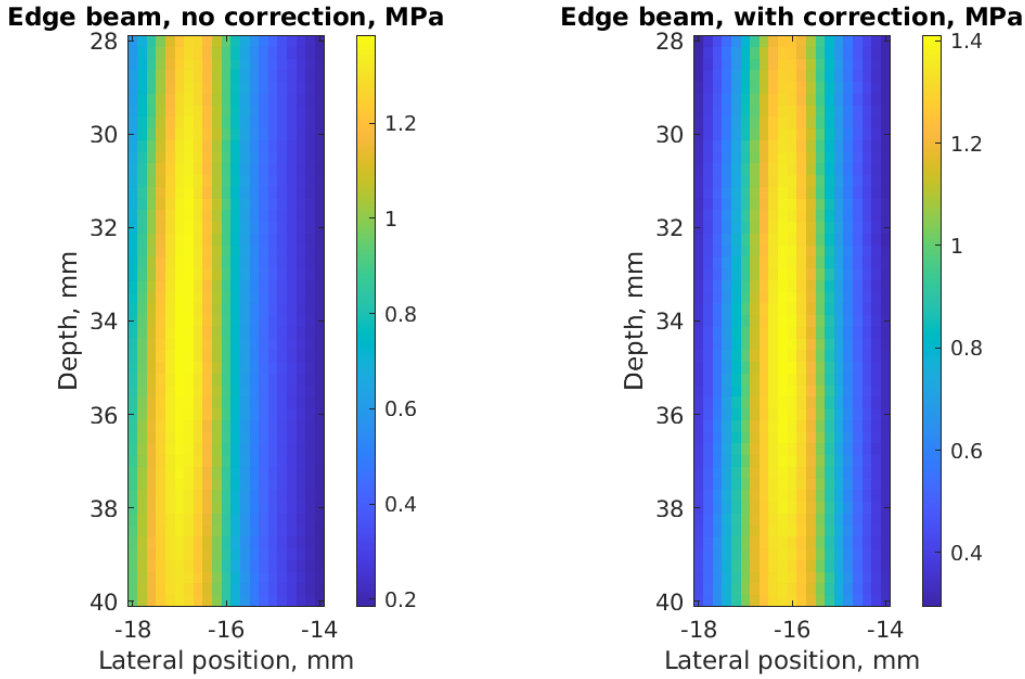

(a) (b)

Figure 3: Transmit delay deviations, measured during transducer characterization.

	Wire at 28 mm	Wire at 50 mm	Wire at 75 mm	Wire at 100 mm
Comm. XDC, default	-47.22	-42.40	-38.38	-34.63
Comm. XDC, corrected	-46.20	-43.82	-40.48	-35.59
Exp. XDC, default	-34.67	-24.15	-21.41	-20.27
Exp XDC, corrected	-37.13	-34.04	-31.15	-28.31

Table 4: Cystic contrast, dB

is not only effective for experimental transducers but also for commercial ones. There was a slight improvement in lateral resolution and cystic contrast when the framework was applied to a commercial transducer (see Figure 5). Currently, the framework only uses one of the output parameters of the transducer characterization approach provided in [1]. The other output parameters, the individual element sensitivity matrix and impulse response matrix, provide additional potential avenues for compensating for transducer imperfections, further improving the image quality.

Although only linear transducers were investigated in this work, the same principle can be applied to convex transducers by replacing the planar reflector with a concentric reflector that matches the center of curvature of the convex transducer. The same principle detailed in this work would apply to finding the geometric model's imperfection and compensating for it.

5. CONCLUSION

The suggested method demonstrates improvements in image quality at no additional computational cost. The only modification is in the transducer element coordinates. Due to that, it is a beneficial and cost-free approach to use in any data acquisition situation. The improvements for commercial transducers manufactured through a well-established process are much less dramatic, as the transducer imperfections in these cases are smaller. The next step in using this method is to apply it to convex array transducers. A complementary approach for transducer model correction, compensating the uneven element amplitude (efficiency, sensitivity) uniformity, will be a subject of future work.

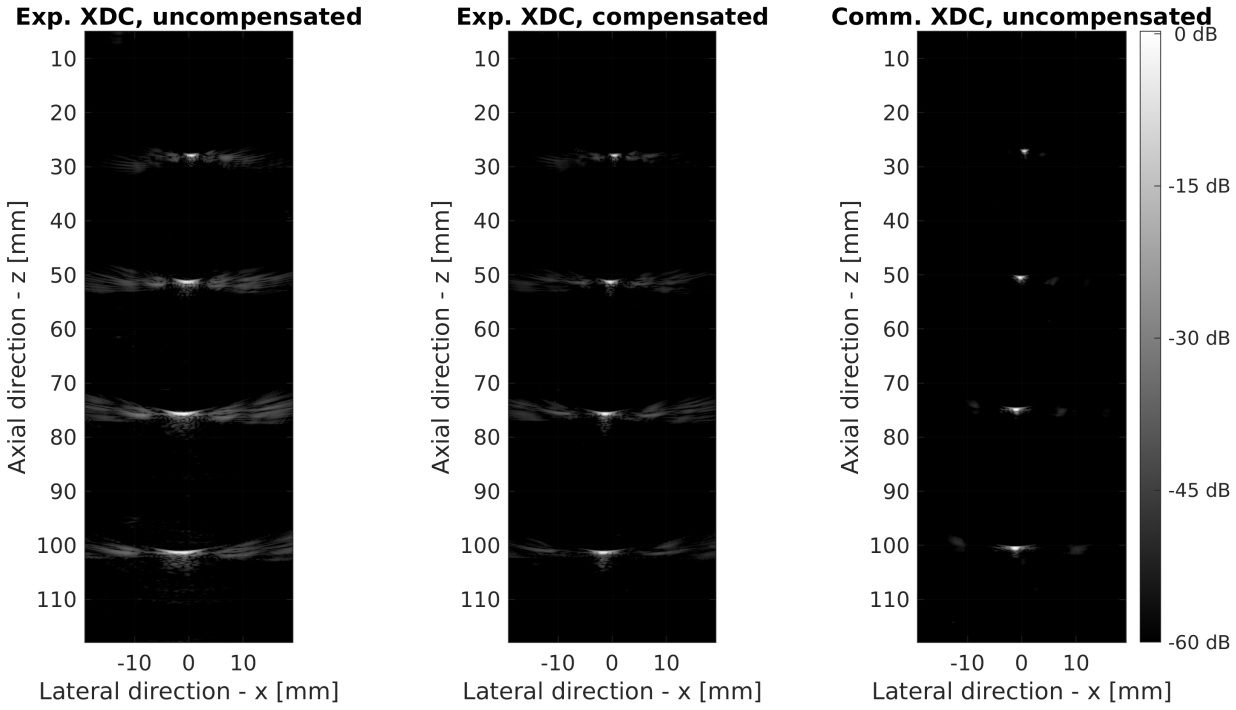

(a) (b) (c)

Figure 4: Images created by generic (a) and corrected (b) beamformation for the experimental array, next to an image made with the commercial array (c).

ACKNOWLEDGMENTS

The work was financially supported by ERC synergy grant 854796 - SURE from the European Research Council.

REFERENCES

[1] Tomov, B. G., Diederichsen, S. E., Thomsen, E. V., and Jensen, J. A., "Characterization of medical ultrasound transducers," in [*Proc. IEEE Ultrason. Symp.*], 1–4 (2018).

[2] McCall, J. R., Chavignon, A., Couture, O., Dayton, P. A., and Pinton, G. F., "Element position calibration for matrix array transducers with multiple disjoint piezoelectric panels," *Ultrason. Imaging* **46**(3), 139–150 (2024). PMID: 38334055.

[3] Jørgensen, L. T., Præsius, S. K., Stuart, M. B., and Jensen, J. A., "Row-column beamformer for fast volumetric imaging," *IEEE Trans. Ultrason. Ferroelec. Freq. Contr.* **70**(7), 668–680 (2023).

[4] Boni, E., Yu, A. C. H., Freear, S., Jensen, J. A., and Tortoli, P., "Ultrasound open platforms for next-generation imaging technique development," *IEEE Trans. Ultrason. Ferroelec. Freq. Contr.* **65**(7), 1078–1092 (2018).

[5] Engholm, M., Bouzari, H., Christiansen, T. L., Beers, C., Bagge, J. P., Moesner, L. N., Diederichsen, S. E., Stuart, M. B., Jensen, J. A., and Thomsen, E. V., "Probe development of CMUT and PZT row–column-addressed 2-D arrays," *Sens. Actuators A: Phys.* **273**, 121–133 (2018).

[6] Jensen, J. A., Tomov, B. G., Haslund, L. E., Panduro, N. S., and Sørensen, C. M., "Universal synthetic aperture sequence for anatomic, functional and super resolution imaging," *IEEE Trans. Ultrason. Ferroelec. Freq. Contr.* **70**(7), 708–720 (2023).

[7] Ranganathan, K. and Walker, W. F., "Cystic resolution: A performance metric for ultrasound imaging systems," *IEEE Trans. Ultrason. Ferroelec. Freq. Contr.* **54**(4), 782–792 (2007).

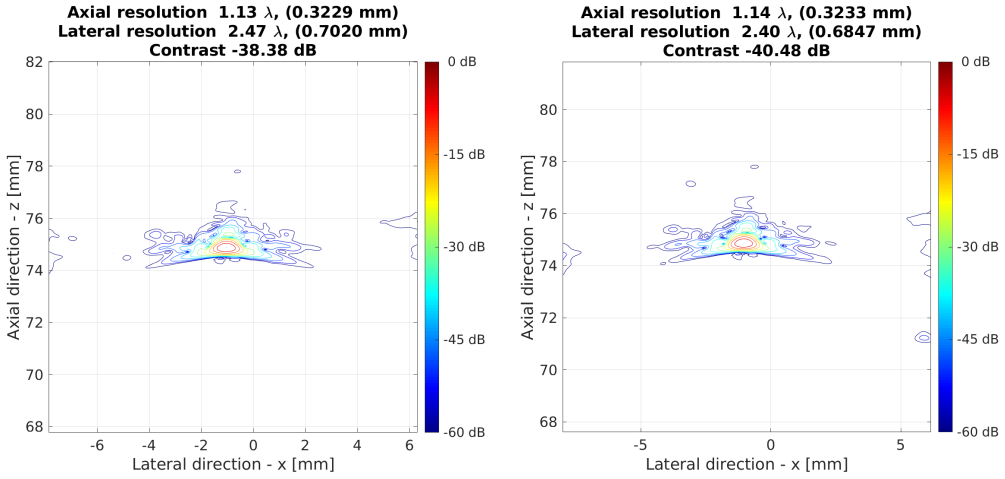

(a) (b)

Figure 5: Contour plots of the image of the third wire, created using generic (a) and corrected (b) geometry model for the commercial array.

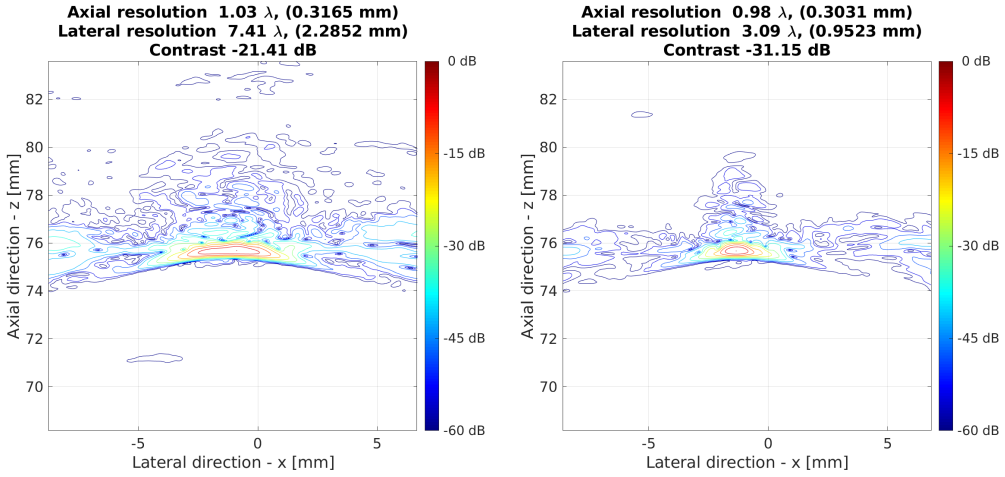

(a) (b)

Figure 6: Contour plots of the image of the third wire, created using generic (a) and corrected (b) geometry model for the experimental array.